Int. J. Heat Mass Transfer. Vol. 36, No. 3, pp. 823–829, 1993
Printed in Great Britain

0017-9310/93 $6.00 + 0.00
Pergamon Press Ltd

TECHNICAL NOTE

Spectral analysis of wall turbulence with photolithography devised electrochemical probes

C. DESLOUIS, F. HUET, S. ROBIN and B. TRIBOLLET
UPR 15 du CNRS 'Physique des Liquides et Electrochimie', Université Pierre et Marie Curie, tour 22, 4 place Jussieu, 75252 Paris Cedex 05, France

(*Received* 5 *October* 1991)

INTRODUCTION

AN INCREASING attention has been devoted in the recent years to the study of wall turbulence mainly because the succession of events which lead to the fully developed turbulence takes place near the wall. Unfortunately, only few experimental methods can be successfully used in that region. Among them, the electrochemical method appears as the most appropriate, enabling to measure the velocity gradient at the wall, over a distance from the wall not exceeding some micrometers [1–3].

The analysis of turbulent fluctuations can be done in the framework of a linear theory if the ergodicity and the stationarity of the time-dependent fluctuations can be assumed.

In that case, it is known that the power spectral density (psd) W_I of the limiting diffusion current I, and the psd W_α of the wall velocity gradient α, are linked through the following relationship [4, 5]:

$$W_I(f) = |\mathscr{H}(f)|^2 W_\alpha(f) \qquad (1)$$

where $\mathscr{H}(f)$ is the transfer function between I and α, depending on the frequency f.

A correct use of equation (1) needs two conditions:

(i) The transfer function $\mathscr{H}(f)$ must be accurately known in the whole frequency range. As a matter of fact, as attenuation takes place at moderate frequencies in a liquid, due to the high Schmidt number value ($Sc \cong 10^3$), the calculation of W_α from the ratio $W_I/|\mathscr{H}(f)|^2$ is particularly sensitive to the precision on $\mathscr{H}(f)$ in high frequencies.

(ii) Both the time-depending fluctuations and the average value must be uniform over the whole probe surface, a condition generally designated as homogeneity. As turbulence is characterized by a distribution of scales (in time or length), homogeneity is ensured only when the smallest length scale investigated is larger than the probe dimension.

The calculation of $\mathscr{H}(f)$ was performed in earlier works either analytically [6–8] or numerically [9–11]. The former expressions corresponded to the local transfer function based on the local current density instead of the overall current integrated over the probe surface. An asymptotic behavior in $f^{-3/2}$ was then predicted [7, 8]. The more recent calculations carried out for a real probe (i.e. of the overall current) give a f^{-1} dependence [9–11] which has been experimentally confirmed with two modulated flows: the rotating disk [11] or the cone and plate device [12].

In contrast, the limitation entailed by the homogeneity condition is not yet clearly understood and meets some experimental considerations. As a matter of fact, electrochemical probes are prepared so far in a rather tedious way by embedding a wire or a thin sheet of metal and sealing it with an epoxy resin in an insulating material. The surface is then polished so that only the cross-section of the metal acts as the electrode surface.

Checking the homogeneity condition with this method of preparation raises some geometrical difficulties such as the contour definition of the probe or the crevice formation between the metal and the insulator. In addition, the probe size cannot be too small because those parasitic effects become larger.

To overcome this problem, photolithography, which is a routine technique for preparing integrated circuits, was chosen as a new method for preparing microelectrodes. By this way, it is possible to obtain microelectrodes of various shapes with accurate dimensions.

The primary aims of this work were:

(1) Determination of the homogeneity domain, at least in the inertial range of turbulence, by an adequate choice of the probe geometry and dimensions.

(2) Determination of the velocity gradient spectrum from the limiting diffusion current spectrum and its analysis under conditions fulfilling the theoretical requirements.

The experiments were conducted on a rectangular channel approaching an ideal 2-D geometry: this allowed to verify some hypotheses related to the turbulent regime in the channel.

PRINCIPLE OF THE ELECTROCHEMICAL METHOD

The mass fluxes are measured by means of a redox reaction $ox + ne^- \rightleftarrows red$, exchanging electrons with a metallic electrode flush with the wall (x, z plane in Fig. 1). When a high overvoltage (positive or negative) is applied to the electrode, one of the oxidized or reduced species is consumed at an infinitely fast rate at the metal/liquid interface, so that a perfect mass sink is obtained at the wall ($C_W = 0$). On the remaining insulating area of the wall, one has $\partial C/\partial y|_0 = 0$.

The limiting diffusion current density i measured in these conditions is proportional to the mass transfer rate J as follows:

$$i = nFJ \qquad (2)$$

where J is defined by the first Fick law

$$J = -D\left.\frac{\partial C}{\partial y}\right|_0 \qquad (3)$$

F is the Faraday number ($F = 96\,500$ C/equiv.), and D the molecular diffusion coefficient.

In this work, the benzoquinone/hydroquinone redox

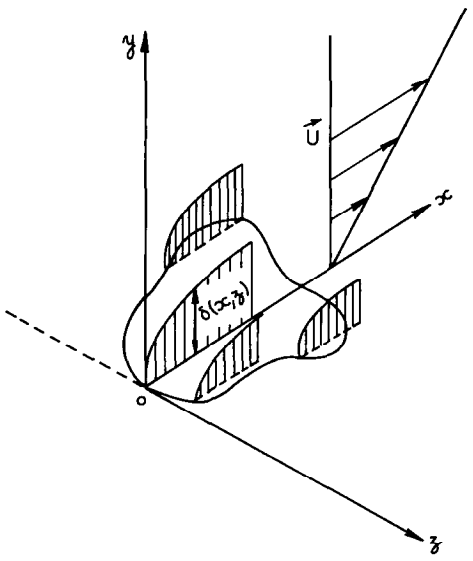

FIG. 1. Developing concentration boundary layer $\delta(x, z)$ over a microelectrode of arbitrary shape in the x, z plane, placed in a one-dimensional flow U along the x-direction.

couple has been used

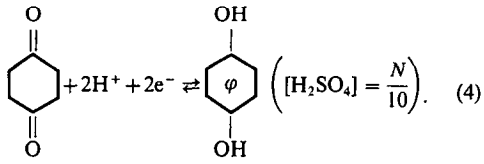

$$\left([H_2SO_4] = \frac{N}{10}\right). \quad (4)$$

MASS TRANSFER ANALYSIS

Consider a probe of an indifferent shape, flush with an insulating (x, z) plane (see Fig. 1). For a fully developed turbulent flow having its mean velocity value $\bar{U}$ along the x-axis, the three time-dependent velocity components are given by:

$$\mathbf{U}\begin{vmatrix} \bar{U}+u \\ v \\ w \end{vmatrix} \quad \text{with} \quad \bar{u} = \bar{v} = \bar{w} = 0$$

where the bars denote time average quantities.

In a liquid, the Schmidt number Sc ($Sc = \nu/D$, ν kinematic viscosity) is so high that the local thickness $\delta(x, z)$ of the concentration boundary layer remains very thin and allows the velocity components to be represented by their first term in a Taylor expansion. Thus

$$\bar{U} = Sy, \quad \begin{matrix} u = \alpha(x,z,t)y \\ v = \beta(x,z,t)y^2 \\ w = \gamma(x,z,t)y \end{matrix} \quad (5)$$

with $\bar{\alpha} = \bar{\beta} = \bar{\gamma} = 0$.

Those velocity fluctuations induce concentration fluctuations

$$C = \bar{C} + c(x, y, z, t)$$

with

$$\bar{c} = 0.$$

The mass balance equation relates the time-dependent concentration field to those velocity components

$$\frac{\partial c}{\partial t} + \mathbf{U}\cdot\nabla C = D\ \Delta C. \quad (6)$$

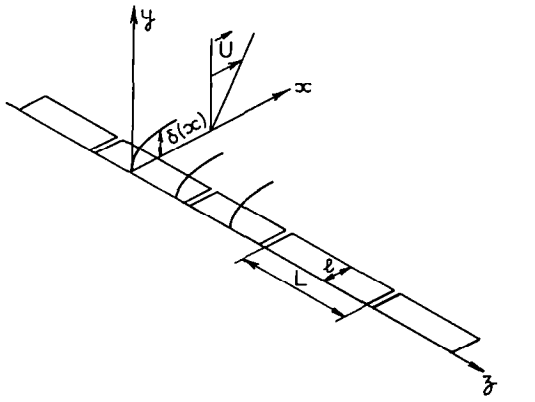

FIG. 2. Rectangular microelectrodes array, sensitive to the x velocity component.

Considering the correlations existing between the fluctuating concentrations and velocities, that is, for example: $\overline{cv} \neq 0$, and removing from equation (6) the stationary solution, one has

$$\frac{\partial c}{\partial t} + \bar{U}\cdot\frac{\partial c}{\partial x} + \mathbf{u}\cdot\nabla\bar{C} + \nabla(c\mathbf{u} - \overline{c\mathbf{u}}) = D\Delta c \quad (7)$$

where $\mathbf{u}$ has three components (u, v, w).

Since only the x velocity fluctuations are studied in this work, the electrode shape must be defined accordingly.

By using a set of rectangular electrodes separated by a very thin insulating gap (see Fig. 2), the first and second concentration derivatives with respect to z are eliminated. This is not true for the two edge electrodes which play the role of guard electrodes.

When the microelectrode width l is small enough (Fig. 2), the concentration profile cannot develop far from the wall since: $\delta(x) \propto x^{1/3}$ [13], and the effect of the normal component v, varying as y^2, is negligible on mass transport [14], A drastic damping close to the wall is also observed for the quadratic terms which cause turbulent diffusion: the quadratic term $\overline{cv}$ can be represented as a turbulent flux $D_T\cdot(\partial\bar{C}/\partial y)$, and the models proposed to predict the expression of D_T, the turbulent diffusion coefficient, are generally written as

$$D_T/\nu \propto (y^+)^n$$

with $3 \leqslant n \leqslant 4$ and $y^+ = yV_0/\nu$, where V_0 is the friction velocity.

There is also a lower limit to l below which diffusion in the mean flow direction becomes significant: this limit, determined by Ling, is such that [15]:

$$Sl^2/D \cong 5000.$$

When the homogeneity condition is assumed to be verified (i.e. for an electrode of small area), S and α are independent of x and z.

With all the above simplifications, including homogeneity, equation (7) can be written as

$$\frac{\partial c}{\partial t} + Sy\frac{\partial c}{\partial x} - D\frac{\partial^2 c}{\partial y^2} = -\alpha y\frac{\partial\bar{C}}{\partial x}. \quad (8)$$

The time average solution was given earlier by Levêque [15]

$$\bar{C} = \frac{C_\infty}{3^{2/3}\Gamma(4/3)}\int_0^{y/\delta(x)} \exp\left(-\frac{\eta^3}{9}\right)d\eta \quad (9)$$

where C_∞ is the solute concentration in the bulk and $\delta(x) = (D/Sx)^{1/3}$. The local value of the diffusion boundary layer is $3^{2/3}\Gamma(4/3)\delta(x)$.

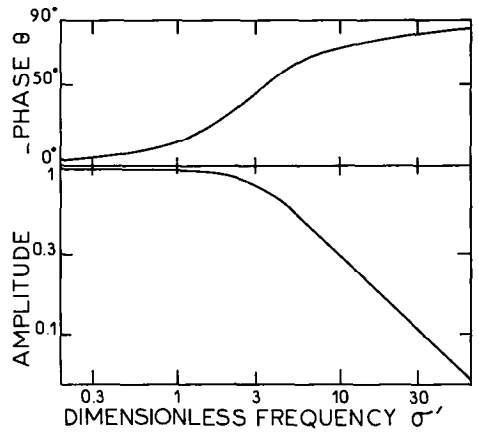

FIG. 3. Normalized transfer function $H(\sigma')/H(0)$ between the mass transfer rate and the velocity gradient ($\sigma' = \omega(l^2/DS^2)^{1/3}$) defined by equations (12) and (13).

In the Nernst approximation, the limiting current is given by

$$I = 0.807\, nFD^{2/3}C_\infty S^{1/3}l^{2/3}L. \tag{10}$$

The right-hand side term in equation (8) represents the velocity perturbation which can be:

(i) either imposed externally as a sinusoidal modulation of the laminar flow at frequency $\omega/2\pi$;
(ii) or induced internally by turbulence.

In both situations, the Fourier transform of equation (8) leads to

$$j\omega\tilde{c}(\omega) + Sy\frac{\partial\tilde{c}(\omega)}{\partial x} - D\frac{\partial^2\tilde{c}(\omega)}{\partial y^2} = -\tilde{\alpha}(\omega)y\frac{\partial\bar{C}}{\partial x}. \tag{11}$$

The tilded quantities denote Fourier transforms.

The solution of this equation in case (i) can be expressed in terms of a transfer function $H(\omega)$ between the mass transfer rate $\tilde{J}(\omega)$ and $\tilde{\alpha}(\omega)$.

H was calculated in [11] vs a dimensionless frequency $\sigma' = \omega(l^2/DS^2)^{1/3}$:

- in low frequency ($\sigma' \leqslant 6$):

$$\frac{|H(\sigma')|}{|H(0)|} = (1 + 0.056\sigma'^2 + 0.00126\sigma'^4)^{-1/2} \tag{12}$$

$$\arg H = -\arctan[0.276\sigma'(1 + 0.02\sigma'^2 - 0.00026\sigma'^4)]$$

- in high frequency ($\sigma' > 6$):

$$\frac{H(\sigma')}{H(0)} = \frac{3.715}{j\sigma'} - \frac{3.99}{(j\sigma')^{3/2}}. \tag{13}$$

The variation of $H(\sigma')$ is given in Fig. 3.

Now, if the transfer function $\mathscr{H}(\omega)$ defined by equation (1) is considered

$$\tilde{I}(\omega) = \mathscr{H}(\omega)\tilde{\alpha}(\omega) \tag{14}$$

$\tilde{I}(\omega)$ being directly proportional to $\tilde{J}(\omega)$ (equation (2)), the transfer function $\mathscr{H}(\omega)$ is also proportional to $H(\omega)$ and $\mathscr{H}(\omega)/\mathscr{H}(0) = H(\omega)/H(0)$.

$\mathscr{H}(0)$ is equal to $(1/3)(\bar{I}/S)$, the derivation of $\bar{I}$ with respect to S (equation (10)). Then equation (14) becomes

$$\tilde{I}(\omega) = \frac{1}{3}\frac{\bar{I}}{S}\frac{H(\omega)}{H(0)}\tilde{\alpha}(\omega) \tag{15}$$

$$\mathscr{H}(\omega) = \frac{1}{3}\frac{\bar{I}}{S}\frac{H(\omega)}{H(0)}. \tag{16}$$

Consider now the second situation. One can write also equation (14) where now $\tilde{\alpha}(\omega)$ is a random function induced by turbulence and $\mathscr{H}(\omega)$ is the same transfer function as above (equation (16)). Therefore

$$|\tilde{I}(\omega)|^2 = |\mathscr{H}(\omega)|^2 \cdot |\tilde{\alpha}(\omega)|^2. \tag{17}$$

As $|\tilde{I}(\omega)|^2$ and $|\tilde{\alpha}(\omega)|^2$ are proportional to the psd W_I and W_α, one finds again equation (1). W_I is measured experimentally with a Fourier analyzer, $\mathscr{H}(\omega)$ is theoretically known from equations (12), (13) and (16); thus W_α can be deduced.

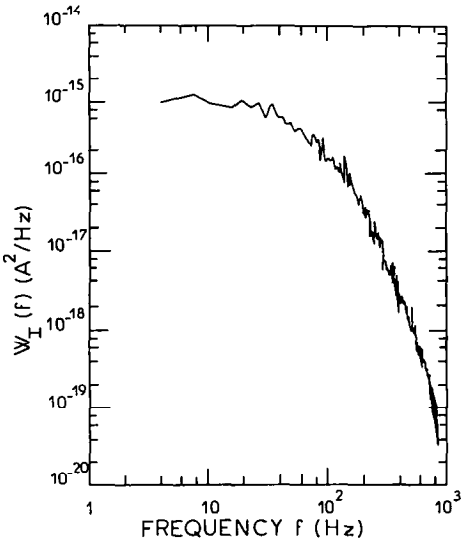

FIG. 4. (a) psd of the limiting current fluctuations for a microelectrode with a length $L = 200\ \mu$m. Reynolds number $Re = 15\,800$; $Sc = 1130$. (b) psd of the wall velocity gradient fluctuations deduced from the data of Fig. 4(a) by applying equation (1).

PREPARATION OF MICROELECTRODES: PHOTOLITHOGRAPHY

The microelectrode designs are drawn at scale 100. A first reduction of 10 is taken on a high grade film on which the electrical contacts are added, and after a second reduction of 10, the photographic mask at scale 1 is obtained.

On a GaAs substrate doped with chromium (resistivity:

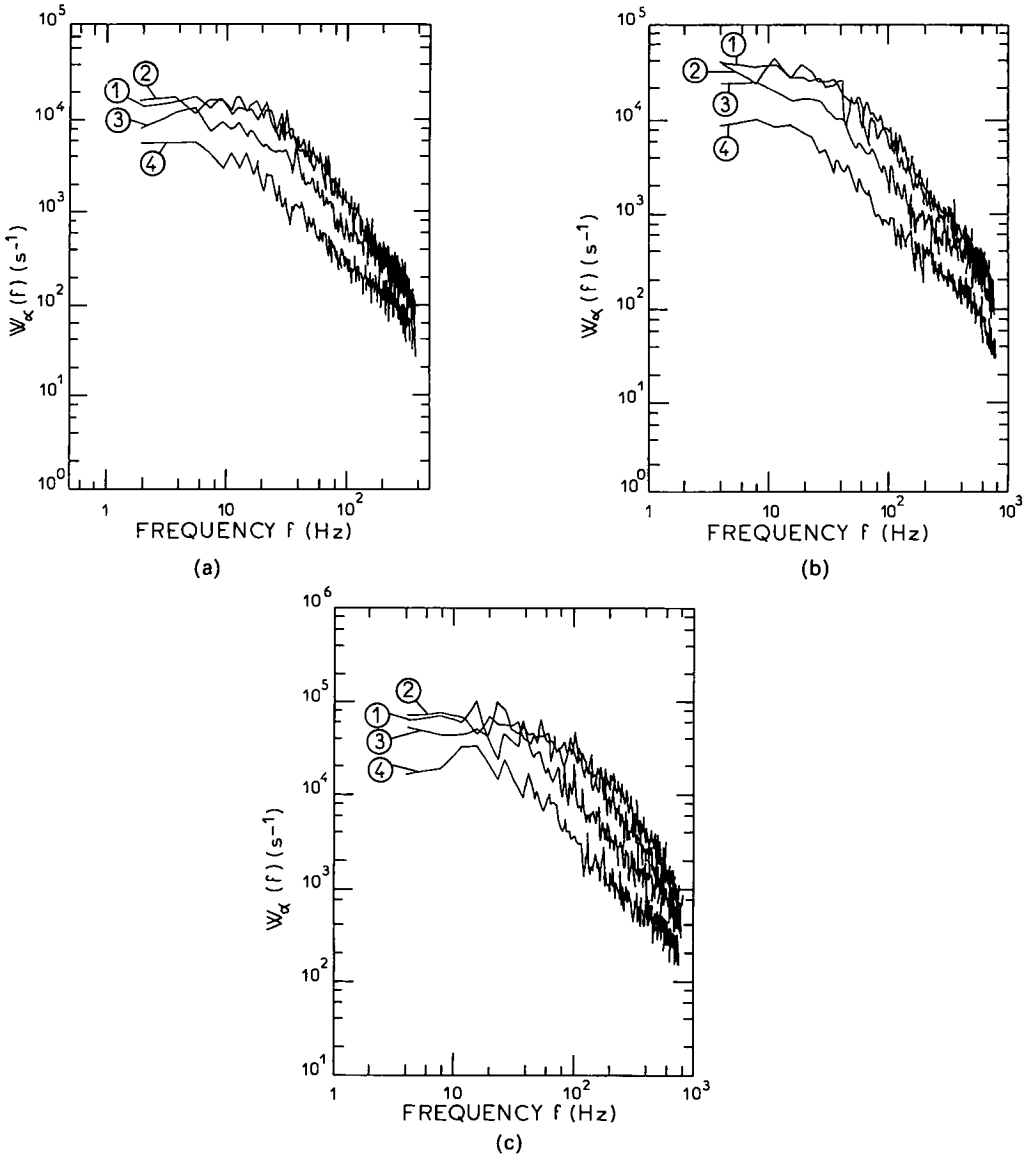

FIG. 5. psd of the wall velocity gradient fluctuations deduced from equation (1) for different Reynolds numbers and different electrode lengths. $L = 100\ \mu m$ (1); $390\ \mu m$ (2); $1000\ \mu m$ (3); and $2485\ \mu m$ (4). (a) $Re = 11\,250$; (b) $Re = 15\,800$; (c) $Re = 24\,490$.

$10^8\ \Omega$ cm), a photosensitive resin layer is spread with a constant thickness of $0.8\ \mu m$. The photographic mask, which is an emulsion on a flexible material, is placed against the GaAs wafer with the resin. The resin is then sunbathed with a U.V. mercury lamp and finally developed, leaving bare the GaAs portions corresponding to the electrode area and the electrical contacts. Before the chemical deposition of gold [16], the bare surface of GaAs is activated with a solution of palladium chloride in acidic medium. The gold layer thickness is 1500 Å. The sunbath technique with U.V. is used for a second level of masking in order to cover with insulated resin the electrical contacts and to leave only the active part of the microelectrodes in contact with solution.

EXPERIMENTAL SET-UP

The experiments were conducted on a fully turbulent flow in a two-dimensional rectangular channel. This channel (2.85 m long, 12 cm wide and 1.2 cm high) was placed between two tanks ($\cong 200$ l). The flow through the channel was achieved by imposing a pressure in one tank, the other one being open to the atmospheric pressure. The electrochemical section was located at 2 m downstream of one tank so as to ensure fully developed flow conditions. The measurement was therefore performed in one direction, the fluid being recirculated toward the upstream tank after each pass. The pressure was controlled by a pneumatic feedback device in order to stabilize the flow rate value within $\pm 0.5\%$. The controlled voltage of the microelectrode sets to zero the concentration value of the reacting species at the wall. The diffusion current in the electrolysis cell was measured by means of a current follower.

In order to compare the size effect of different microelectrodes, the signals corresponding to all the microelectrodes have been recorded simultaneously for ensuring the same flow conditions.

The spectrum analyzer used (Hewlett Packard 5451C) allows the signal to be analyzed in a wide frequency range (10^{-4}–5×10^4 Hz). In these experiments, the useful range was

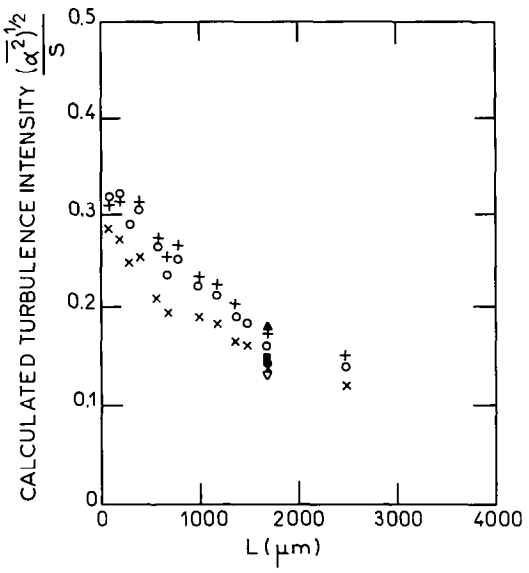

FIG. 6. Apparent turbulent intensity at the wall deduced from Fig. 5, as function of the electrode length L. Gold electrodes obtained by photolithography ($L = 23$ μm): $Re = 11250$ (+); 15800 (○); 24490 (×). Platinum electrodes obtained from a sheet of $l = 50$ μm: $Re = 10330$ (△); 13830 (▲); 22240 (●); and 24325 (▽).

limited to 10^{-1}–10^{3} Hz: the higher limit was imposed by the instrumentation background noise and the lower limit by the tank volume imposing the acquisition time for a given flow rate.

TIME CORRELATIONS: ANALYSIS OF THE POWER SPECTRAL DENSITY (PSD)

As mentioned above, the one-dimensional spectrum W_x of the longitudinal wall velocity gradient is obtained from the spectrum W_I of the limiting diffusion current fluctuations by applying equation (1) with $\mathscr{H}$ defined from equations (12), (13) and (16). As an example, a psd of the limiting diffusion current fluctuations and the deduced psd of the wall velocity gradient fluctuations are shown respectively in Figs. 4(a) and (b). In the following, the W_x psd will be directly given.

Five rectangular microelectrodes, of same width 25 μm and different lengths between 100 and 1000 μm, have been prepared by the photolithography technique. The responses for other lengths can also be obtained by summing the recorded signals of different contiguous microelectrodes, the effect of the insulating gap ($\cong 5$ μm) being negligible. So, from the five currents recorded simultaneously, it is possible to deduce the currents for 15 lengths.

The W_x psd corresponding to $L = 100$ or 390 μm are identical for $Re = 11250$ (Fig. 5(a)) or 15800 (Fig. 5(b)) and slightly separated for $Re = 24490$ (Fig. 5(c)).

When the electrode length increases, the psd decreases especially in the low frequency domain. As there is only a small decrease in the high frequency domain, the slope of the spectrum increases with L.

The relative turbulence intensity $(\bar{\alpha}^2)^{1/2}/S$ is given in Fig. 6 as function of the microelectrode length. For the low L values, the turbulence intensity is in good agreement with the experimental value 0.3 obtained by other techniques (hot wire anemometry, laser Doppler anemometry) at some distance from the wall and then extrapolated [17]. In particular, for $L = 100$ μm, this intensity is equal to 0.30 ± 0.02.

In Fig. 7, $(\bar{\alpha}^2)^{1/2}/S$ is also given vs a dimensionless length $L^+ = LV_0/\nu$. The relative intensity of turbulence is constant and equal to 0.3 below $L^+ \cong 20$. This value of 20 must correspond approximately to the transverse turbulent length scale.

A quantitative analysis was developed by Uberoi and Kovasznay [18] who proposed a correction factor to treat the behavior of a hot wire anemometer with a length larger than the size of the smallest eddies. A ratio between the measured turbulence intensity and the actual one was obtained under the following form:

$$\frac{\overline{u^2}_{\text{measured}}}{\overline{u^2}_{\text{true}}} = \frac{\Lambda^+_{fz}}{L^+} \operatorname{erf}\left(\frac{L^+\sqrt{\pi}}{2\Lambda^+_{fz}}\right). \tag{18}$$

This analysis was based on the hypothesis of an homogeneous and isotropic turbulence but these conditions are, a priori, not fulfilled with this flow geometry and close to a wall. In addition, the three integral correlation lengths, Λ^+_{fx}, Λ^+_{fy} or Λ^+_{fz}, must be very different. Whereas Λ^+_{fx} had been previously measured around 480 [19], Λ^+_{fz} cannot be clearly defined by the integral relation:

$$\Lambda^+_{fz} = \int_0^{\infty} f(z^+)\,dz^+$$

because the longitudinal correlation function $f(z^+)$ becomes negative for large z^+ values [20]. Following the data obtained by Campbell and Hanratty [21], it is possible to estimate an upper limit of Λ^+_{fz} of 35 by writing

$$\Lambda^+_{fz} = \int_0^{z_1^+} f(z^+)\,dz^+$$

z_1^+ corresponding to the value where f becomes negative.

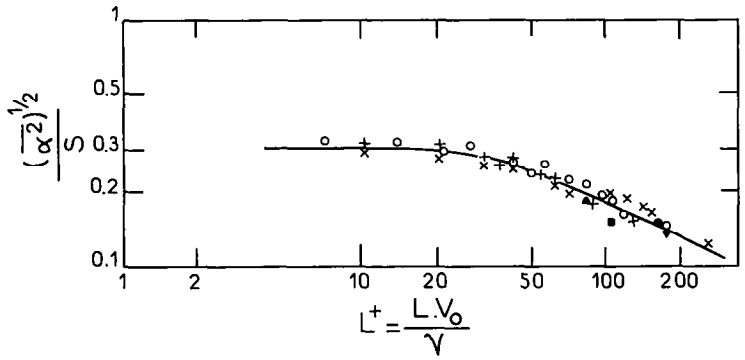

FIG. 7. Same data as in Fig. 6 reported vs the dimensionless electrode length $L^+ = LV_0/\nu$ where V_0 is the friction velocity. Curve in full line represents the equation of Uberoi and Kovasznay [18], equation (18).

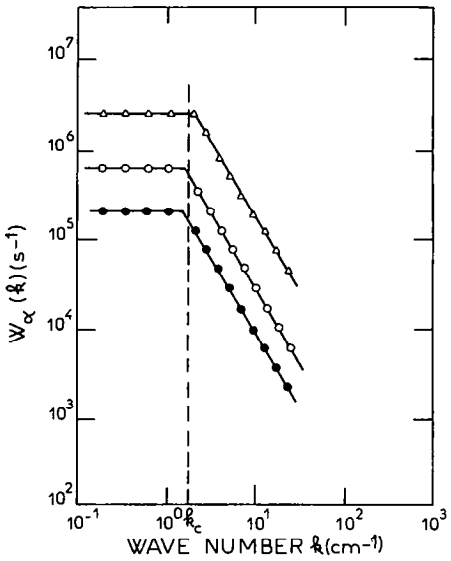

FIG. 8. psd of the wall velocity gradient fluctuations as function of the wave number. $L = 200$ μm, $Sc = 1130$. $Re = 11\,250$ (●); 15 800 (○); 24 490 (△).

This Λ_{fc}^{+} value introduced in equation (18) gives a very good fit to the experimental data (Fig. 7).

In fact, no correction is necessary if the dimensionless length of the electrochemical probe is smaller than 20. When L^+ is larger than 20, the general equation (18) must be applied. The data presented further obey the condition $L^+ \leqslant 20$.

Coming back to the psd of Fig. 5, the L^+ value of 20 determined above which ensures homogeneity, is consistent with the indiscernibility of the spectra at all frequencies for small length values. In fact, L^+ around 20, considering an order of magnitude of 10 cm s^{-1} for V_0, yields $L \cong 200$ μm. Therefore, the velocity gradient spectrum of Fig. 4(b) correctly describes the aspect of the inertial range, which appears as a linear portion in the high frequency range with a slope -1.65 ± 0.1.

This value is in good agreement with the second hypothesis of Kolmogorov's theory of isotropic turbulence, revealing the existence of an inertial subrange near the wall for which a concept of local isotropy is thus likely to be applicable.

In the experimental velocity gradient spectra, a substantial part of the inertial subrange is observed but the dissipation range (Taylor scale) at higher frequencies, where the spectrum should fall off more rapidly, was not observed because of a limitation due to background noise of instrumentation.

Considering the large structures associated to the low frequency plateau, the Taylor hypothesis can be used, assuming that the disturbances are transported with the flow rate V without distortion. Their wave number k is thus related to frequency by

$$k = 2\pi f / V.$$

The velocity gradient spectra are shown as a function of the wave number for different Reynolds numbers in Fig. 8. It is concluded that, in this regime, the cut-off wave number k_c is independent of the Reynolds number and equal to:

$$k_c = 1.9 \pm 0.3\,\text{cm}^{-1}.$$

This value corresponds to a wavelength of 3.3 cm which is about 5.5 times larger than the half-height of the channel (0.6 cm). As this dimension is a limit to the size of the largest vortices, this accounts for a vortex stretching in the mean flow direction as already assumed in ref. [22].

CONCLUSION

In conclusion, it has been shown that the polarographic technique applied to photolithography devised microelectrodes becomes a really powerful tool for quantitative analysis of flows in the wall vicinity. As specific advantages, it has been pointed out that prescribed geometry and precise dimensions can be obtained so that a close agreement with theoretical requirements is ensured.

The homogeneity domain for longitudinal velocity fluctuations was found to be consistent with a transverse turbulent length scale around 20. In the inertial range, a Kolmogorov type law $f^{-5/3}$ was found.

The transverse turbulent length scale being smaller than the longitudinal turbulent length scale, the 20 value can be used in order to determine the diameter of circular or bicircular electrode. One can now expect to obtain, with a much better accuracy than before, the one-dimensional spectrum of the velocity fluctuations in the transverse direction and the space correlations in the longitudinal and transverse directions.

REFERENCES

1. C. S. Lin, E. B. Denton, H. S. Gaskill and G. L. Puttmann, Diffusion-controlled electrode reactions, *Ind. Engng Chem.* **43**, 2136–2143 (1951).
2. L. P. Reiss and T. J. Hanratty, Measurement of instantaneous rates of mass transfer to a small sink on a wall, *A.I.Ch.E. Jl* **8**, 245–248 (1962).
3. T. J. Hanratty and J. A. Campbell, Measurement of wall shear stress. In *Fluid Mechanics Measurements* (Edited by R. J. Goldstein), p. 559. Hemisphere, Washington, D.C. (1983).
4. V. E. Nakoryakov, O. N. Kashinsky and B. K. Kozmenko, Electrochemical method for measuring turbulent characteristics of gas–liquid flows. In *Measuring Techniques in Gas–Liquid Two-phase Flows*, IUTAM Symposium, Nancy, France, pp. 695–721 (1983).
5. C. Deslouis, B. Tribollet and L. Viet, The correlation between momentum and mass transfer for a turbulent or periodic flow in a circular pipe by electrochemical methods, 4th Int. Conf. on Physicochemical Hydrodynamics, *Ann. NY Acad. Sci.* **404**, 471–473 (1983).
6. Yu. Ye. Bogolyubov, P. I. Geshev, V. Y. Nakoryakov and I. A. Ogorodnikov, Theory of electrodiffusion method applied to the characteristic spectra measurement in turbulent flow, *Prikl. Mekh. Teckln. Fiz.* **4**, 112 (1972).
7. M. A. Vorotyntsev, S. A. Martemjanov and B. M. Grafov, Temporal correlation of current pulsations at one or several electrodes: a technique to study hydrodynamic fluctuation characteristics of a turbulent flow, *J. Electroanal. Chem.* **179**, 1–23 (1984).
8. G. Fortuna and T. J. Hanratty, Frequency response of the boundary layer on wall transfer probes, *Int. J. Heat Mass Transfer* **14**, 1499–1507 (1971).
8. Z. X. Mao and T. J. Hanratty, The use of scalar transport probes to measure wall shear stress in a flow with imposed oscillations, *Exp. Fluids* **3**, 129–135 (1985).
10. V. E. Nakoryakov, A. P. Burdukov, O. N. Kashinsky and P. I. Geshev, *Electrodiffusion Method of Investigation into the Local Structure of Turbulent Flows* (Edited by V. G. Gasenko). Novosibirsk (1986).
11. C. Deslouis, O. Gil and B. Tribollet, Frequency response of electrochemical sensors to hydrodynamic fluctuations, *J. Fluid Mech.* **215**, 85–100 (1990).
12. C. Deslouis, O. Gil and B. Tribollet, Frequency response of electrochemical sensors in a cone-and-plate modulated flow, *Int. J. Heat Mass Transfer* **33**, 2525–2532 (1990).
13. M. A. Levêque, Les lois de la transmission de chaleur par convection, *Ann. Mines* **13**, 201–299, 305–362, 381–415 (1928).

14. B. M. Grafov, S. A. Martemjanov and L. N. Nekrasov, *The Turbulent Diffusion Layer in Electrochemical Systems*. Nauka, Moscow (1990).
15. S. C. Ling, Heat transfer from a small isothermal span wire strip on an insulated boundary, *Trans. ASME C, J. Heat Transfer* **85,** 230–236 (1963).
16. Y. Okinaka, An electrochemical study of electroless gold-deposition reaction, *J. Electrochem. Soc.* **120,** 739–744 (1973).
17. H. Eckelmann, Mitteilungen Max-Planck-Inst. für Strömungsforschung, Göttingen, No. 48 (1970).
18. M. S. Uberoi and L. S. G. Kovasznay, On mapping and measurement of random fields, *Appl. Math.* **10,** 375–393 (1953).
19. K. K. Sirkar and T. J. Hanratty, Relation of turbulent mass transfer to a wall at high *Sc* numbers to the velocity field, *J. Fluid Mech.* **44,** 589–603 (1970).
20. J. O. Hinze, *Turbulence*, p. 43. McGraw-Hill, New York (1975).
21. J. A. Campbell and T. J. Hanratty, Turbulent velocity fluctuations that control mass transfer to a solid boundary, *A.I.Ch.E. Jl* **29,** 215–221 (1983).
22. A. E. Perry and M. S. Chong, On the mechanism of wall turbulence, *J. Fluid Mech.* **119,** 173–217 (1982).